The Astrophysical Journal Letters, 904:L27 (7pp), 2020 December 1 https://doi.org/10.3847/2041-8213/abc9b6
© 2020. The American Astronomical Society. All rights reserved.

The Role of Far-ultraviolet Pumping in Exciting the [O I] Lines in Protostellar Disks and Winds

Ahmad Nemer[1], Jeremy Goodman[1], and Lile Wang[2]
[1] Princeton University, 4 Ivy Lane, Princeton, NJ, USA; anemer@princeton.edu
[2] Center for Computational Astrophysics, Flatiron Institute, 162 Fifth Avenue, New York, NY, USA
Received 2020 August 24; revised 2020 October 27; accepted 2020 November 12; published 2020 December 2

Abstract

We use Cloudy to re-examine excitation of [O I] 6300 Å and [O I] 5577 Å in the X-ray driven photoevaporative wind models of Owen and collaborators, and in more recent magnetothermal models by Wang et al. We find that, at the measured accretion luminosities, the far-ultraviolet (FUV) radiation would populate the upper levels of the oxygen, which would eventually contribute to the [O I] lines. FUV pumping competes with collisions as an excitation mechanism of the [O I] lines, and they each originate from a distinct region in the protostellar disk environment. Consequently, the line strengths and shapes of [O I] 6300 Å and [O I] 5577 Å would be affected by the inclusion of FUV pumping in the radiation transport simulations.

Unified Astronomy Thesaurus concepts: Protoplanetary disks (1300); Atomic physics (2063); Atomic spectroscopy (2099)

1. Introduction

Planets form in protoplanetary disks around young stellar objects (YSOs). The similarities between the timescales predicted for planet formation and disk dispersal in YSOs suggest that the two processes are coupled. Thus, determining the dominant mechanisms for disk dispersal is essential in understanding the formation of planets. A wide range of mechanisms have been suggested to explain how the disks of young stars lose their mass: viscous accretion (e.g., Lynden-Bell & Pringle 1974); photoevaporative disk winds as a result of thermal motion of the gas (Ercolano & Pascucci 2017); planet formation (ALMA Partnership et al. 2015); magneto-hydrodynamic (MHD) winds from small radii (e.g., X-winds; e.g., Shu et al. 2000), or from the broader disk radii (e.g., Konigl & Pudritz 2000). One or more of those mechanisms are responsible for mass loss from protostellar disks, and using emission lines diagnostics presents a way to trace the different dispersal processes.

In the presence of magnetic fields and ionized accretion disks, mass ejection in the form of wind is predicted; probably, the process is complex and involves multiple sub-processes. These could include a magnetocentrifugal or magnetothermal disk wind, with a poloidal magnetic field that is assumed to thread the whole disk; a wind from the inner disk near or within the stellar magnetosphere, such as an X-wind (Shu et al. 2000); or a stellar wind (Ferreira 2013, and references therein). Under the action of the magnetic field, the gas is accelerated to terminal velocities of a few to hundreds of km s^{-1}, forming the slow outflows and the bright jets observed in several young objects (e.g., Frank et al. 2014). As disk and stellar winds extract angular momentum, they can control accretion (e.g., Turner et al. 2014).

Photoevaporation is another key mass-loss process in which the disk surface is heated to temperatures such that the thermal energy of the gas exceeds its gravitational energy so that the gas is able to escape from the system. This effect was first detected in systems where disks are dispersed from around hot stars (e.g., O'dell & Wen 1994). Photoevaporation recently gained more attention due to the detection of high-energy photons (far-ultraviolet (FUV), extreme-ultraviolet (EUV), X-ray) from low-mass stars that could provide the heating required to launch a slow disk wind. Photoevaporative winds are suspected to disperse the disk but, unless magnetized, do not drive accretion (see, e.g., Alexander et al. 2014, and references therein).

The presence of a warm and at least partially ionized disk wind has been confirmed via the observation of a few-km/s blueshift in the profile of the [Ne II]12.8 μm fine structure line (e.g., Güdel et al. 2014, and references therein). Moreover, this line shows high-velocity (HVC) and low-velocity (LVC) components. The HVC of the [Ne II] is clearly associated with jets/outflows (it has been also spatially resolved toward one source; see van Boekel et al. 2009), while the profile and peak velocity of the LVC may be consistent with a photoevaporative disk wind (Pascucci & Sterzik 2009; Baldovin-Saavedra et al. 2012; Sacco et al. 2012; but see also Weber et al. 2020). The line can be reproduced in EUV-driven partially ionized gas models as well as in X-ray-driven models where the gas is largely neutral; these models predict mass-loss rates that differ by 2 orders of magnitude (Ercolano & Owen 2016, hereafter EO16).

More recently, forbidden lines of low-charge and neutral states of heavy elements have provided a potential tool for tracing the slow disk winds. Specifically, the [O I] 6300 Å and [O I] 5577 Å lines have been intensively investigated as wind tracers. Like the [Ne II] 12.8 μm line, the O I lines are observed with an HVC and LVC component where the HVC likely traces a collimated jet outflow. It is unlikely that an EUV-driven wind could produce the observed luminosities, due to insufficient neutral oxygen in the mostly ionized gas. It is suspected that FUV and/or X-ray radiation could provide the physical conditions for collisional excitation of the [O I] ($T_e \sim 6000$ K $n_e > 10^6$ cm^{-3}) without over-ionizing the gas, because of the greater column density (compared to EUV) at which such photons are absorbed. EO16 affirmed that their X-ray photoevaporative models are able to produce the observed luminosities and the line shapes.

There has been debate about the excitation mechanism for the [O I] 6300 Å and [O I] 5577 Å lines. Rigliaco et al. (2013)

brought a new perspective to the observation of the O I LVC. They accurately derived the accretion luminosity for 30 of the Hartigan et al. (1995) stars from H_α emission lines, observed simultaneously with the forbidden lines, which appeared in Beristain et al. (2001). They also used high-resolution spectra to dissect the LVC into a narrow component (NC), which probably traces a photoevaporative wind, and a broad component (BC), which likely traces regions near the surface of the inner disk in Keplerian motion. They observed a correlation between the accretion luminosity and the O I lines' luminosity as well as a correlation between the stellar FUV and the lines' luminosity, but there was no correlation with the X-ray luminosity. This led them to the conclusion that the X-ray photoevaporation models are unlikely to be the only mechanism responsible for exciting these lines. They suggest that the origin of the O I forbidden lines, in addition to photoevaporation, could be due to the dissociation of OH molecules by stellar FUV near the disk surface.

Moreover, Simon et al. (2016) found that both the BC and the NC correlate with the accretion luminosity (which in turn correlates with FUV radiation) over a wide range of accretion luminosities. They also establish a relationship between the FWHM of the BC with the disk inclination and the peak centroid of the line. This brought them to the conclusion that the emission of the BC comes from radii between 0.05 an 0.5 au and that it includes emission from a wind that is broadened by Keplerian rotation. They also observe larger blueshifts for the BC associated with larger accretion luminosities. In view of the gravitational binding energy at these radii, the BC is unlikely to trace a photoevaporative wind but rather an MHD one; but the excitation mechanism is yet to be confirmed. The NC, on the other hand, is predicted to be emitted from larger radii (0.5–5 au) with Keplerian broadening profiles, but the photoevaporative origin of this component is unclear: on the one hand, the lower escape energy needed at these radii would be compatible with a photoevaporative wind, but on the other hand, Simon et al. (2016) did not find the expected anticorrelation between centroid velocity (blueshift) and disk inclination.

Both the observations of Rigliaco et al. (2013) and Natta et al. (2014) invoked inconsistencies between EO10 models and observational data. EO16 have addressed these inconsistencies by modifying their models with the addition of an artificial accretion luminosity, to illuminate the wind but not to drive it, and have handled the effect of neutral-hydrogen collisions on the [O I] lines more carefully. They conclude that their new models are in excellent agreement with the available data, and that the [O I] lines most likely trace photoevaporative winds.

In this Letter we conduct radiation-transfer simulations using Cloudy (Ferland et al. 2017) and the density profiles of hydrodynamic models by Owen et al. (2010) and magnetothermal models by Wang et al. (unpublished) to understand the effect of the accretion luminosity (more specifically the FUV radiation) and the neutral-hydrogen collisions on the thermal excitation of the O I forbidden lines. We also want to investigate the dominant physical process responsible for exciting the [O I] forbidden lines and whether the thermal excitation alone can explain the observed luminosity (as claimed by EO16) or whether there is another physical process, related to the FUV source, that poses a better candidate like OH dissociation (as claimed by Rigliaco et al. 2013 and Gorti et al. 2011) or FUV pumping of the lines by the FUV photons. FUV pumping in this context means excitation to higher bound levels of the oxygen atom by absorption of FUV photons, followed by a cascade of radiative or collisional de-excitations leading to the upper levels of the forbidden lines. We illustrate the effects of pumping in both EO16/10s photoevaporative wind and in Wang et al.'s (unpublished) magnetothermal wind. The goal of this article, however, is to demonstrate the effect of pumping on the [O I] lines, rather than to study whether the lines can distinguish between photoevaporative and magnetothermal winds. We leave the latter for future work, though we note the recent investigation of the subject by Weber et al. (2020).

2. Results

We present the work that we performed, using Cloudy, to simulate the details of the [O I] 6300 Å and 5577 Å line emission from a protoplanetary disk environment. The radiation-transfer simulations were performed following the work of EO16 in an attempt to investigate the excitation mechanisms of the forbidden lines. The code used to produce our results (Cloudy) is different than that used by EO16 (MOCASSIN), and the input parameters differ slightly from theirs, but are still within the range inferred from observations. Hence, the temperature and ionization structure reported in this Letter are somewhat different from those obtained by EO16. Nevertheless, by studying how the line luminosities depend upon the radiation sources and other control parameters, we gain insight into the excitation mechanisms for the [O I] emission. We thank James Owen for supplying the flow field (density, velocity, temperature) underlying Figure 4 of EO16. (The temperature field used by EO16 for the O I emission, however, was not the hydrodynamic one shown in that figure, but rather was recomputed by MOCASSIN (B. Ercolano 2020, private communication).) We approximated EO16's radiation source with four blackbodies with various effective temperatures. We used a blackbody with $T_{\rm eff} = 4250$ K, $M = 0.7 M_\odot$, and $R_* = 2.5\,R_\odot$ to represent the photospheric luminosity ($L_* = 1.83 L_\odot$); another with $T_{\rm eff} = 12000$ K was used to simulate the accretion radiation with a luminosity equal to the stellar luminosity (as in the second row of EO16's Table 1). Finally, we included two more blackbodies to mimic EO16's rather complex X-ray spectral energy distribution (SED): one with $T_{\rm eff} = 10^6$ K, and another with $T_{\rm eff} = 10^7$ K, dividing EO16's X-ray luminosity of 2×10^{30} erg s^{-1} equally between the two. We used the same elemental abundances as reported by EO16. We also include dust grains with different parameters in our model, and we found that dust (besides the input radiation sources) has a significant impact on the luminosity produced. Cloudy is capable only of spherical (or slab) geometries. However, insofar as scattering and optical-depth effects of the [O I] line are unimportant, we can use Cloudy along radial rays through the (non-spherical) wind, each such ray having its own density profile. The gas starts at the illuminated face of the cloud at $r = 1.74 \times 10^{11}$ cm and ends at $r = 40$ au. The density profile that was fed to these Cloudy models was extracted from the results of the hydrodynamic models computed by Owen et al. (2010). The temperature is calculated self-consistently at every zone in Cloudy after solving the statistical equilibrium equations, the ionization balance, and the thermal equilibrium equations. Cloudy includes an extensive network of chemical, collisional,

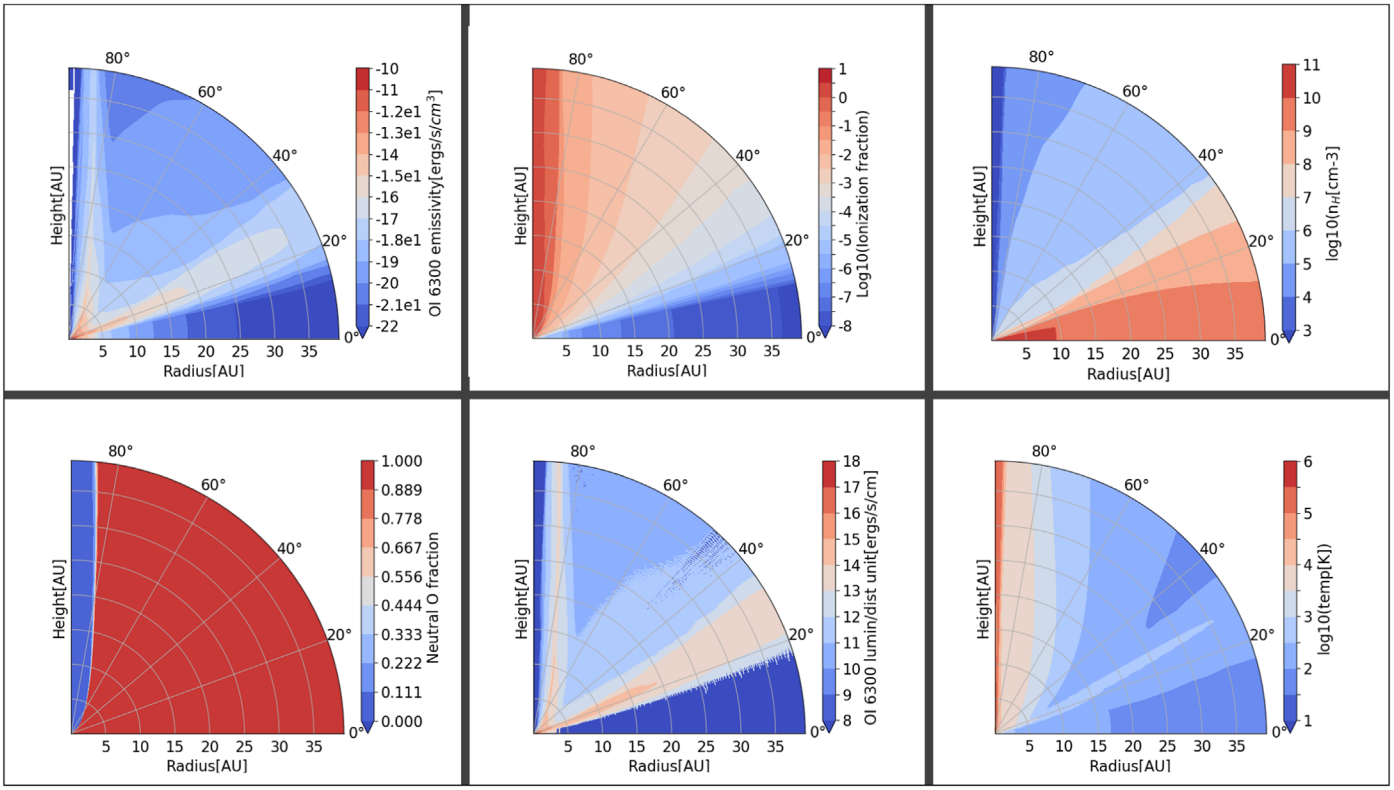

Figure 1. Polar plots of luminosity per distance and emissivity for [O I] 6300 Å along with the ionization fraction, neutral O fraction, temperature and density simulations with the 0.1 μm grains, and using a dust-to-gas ratio of 10^{-4} or a depletion of a factor of 100 to the nominal ISM abundances, using the Owen et al. (2010) model. We note that there are some regions with an ionization fraction $n_e/n_{\rm h} > 1$ due to singly and doubly ionized He ions in those regions.

and radiative processes to accurately obtain solutions for these equilibrium equations. Cloudy also has the possibility to switch on and off some of those various processes.

Below we report the results of the different calculations done to investigate the origin of the [O I] 6300 Å line emission and to reproduce the threshold luminosity $\sim 1 \times 10^{-5} L_{\odot}$ of this line in EO16's models (hereafter the "observed" luminosity), and to investigate the main excitation mechanisms. The calculations were performed on a spherical grid with 1000 linearly spaced points in radius between 0.01 and 40 au, and 241 points uniformly spaced in $\sin\theta \in [0, 1]$. To get the total luminosity, we integrate the line emissions over radius and over one hemisphere in (θ, ϕ), supposing that the disk obscures the emission from the other hemisphere. To avoid the simulation crashing, we extrapolate the the density profile from <0.4 au to the the illuminated face of the cloud, but we exclude emission from radii <0.4 au because this information is missing from the data supplied by Owen et al. (2010).

We varied the size and types of grains used in our models to understand the effect they have on the O I 6300 line emission. We tried models without grains, different abundances of interstellar medium (ISM) dust grains (as used by EO16), different types of polycyclic aromatic hydrocarbon (PAH) grains, and different grain sizes. Most models of Class-II objects postulate a reduction of the dust-to-gas ratio by factors of 10–1000 or more below the nominal ISM value (10^{-2}) in the upper layers of the disk (and in the wind, if any). We investigated the effects of reducing the dust by various factors, this factor being constant throughout a given model—even at the disk midplane. The result was that the less dust, the higher the luminosity of the forbidden lines; but this was mainly due to emission from near the midplane, which in reality should be enhanced in dust if the depletion of the upper layers is due to settling (D'Alessio et al. 2006). We chose a dust-to-gas ratio of 10^{-4} in our key models. We found that some of these models were able to produce the observed luminosity of the [O I] 6300 Å line. In the models that were able to reproduce the observed luminosities for the O I 6300 and 5577 Å lines, their ratio was closer (∼12) to the observed ratio (1–15) than in the models that did not match the observed luminosities (∼45). In our fiducial model Figure 1 (where we use 0.1 μm dust grains), the emission mainly came from two distinct regions. One is a strip that extends along the ionization front from small radii (<0.5 au) to high altitudes (40 au) above the disk, roughly in agreement with EO16; this emission is collisionally excited due to the presence of electrons, a suitable temperature (∼5000 K), and an abundance of neutral oxygen. The other region extends above the surface of the disk and then flares up to an angle of about 60° from the pole. In both regions most of the emission comes from radii less than 3 au. As can be seen there is an extended region beyond the ionization front that includes some emission of the [O I] 6300 Å line. In this region, the temperature is still appropriate for the thermal excitation of the O I line, the gas is mostly neutral, but the electron abundance (relative to H) is a few percent as can be seen from Figure 1. The emission is only a small fraction of the emission from the region along the ionization front.

We turn off the FUV pumping for the fiducial model to find that the emission along the ionization front persists, but the emission from the region above the surface of the disk disappears (Figure 2). (Cloudy has an option to exclude FUV pumping from the solution of the statistical equilibrium

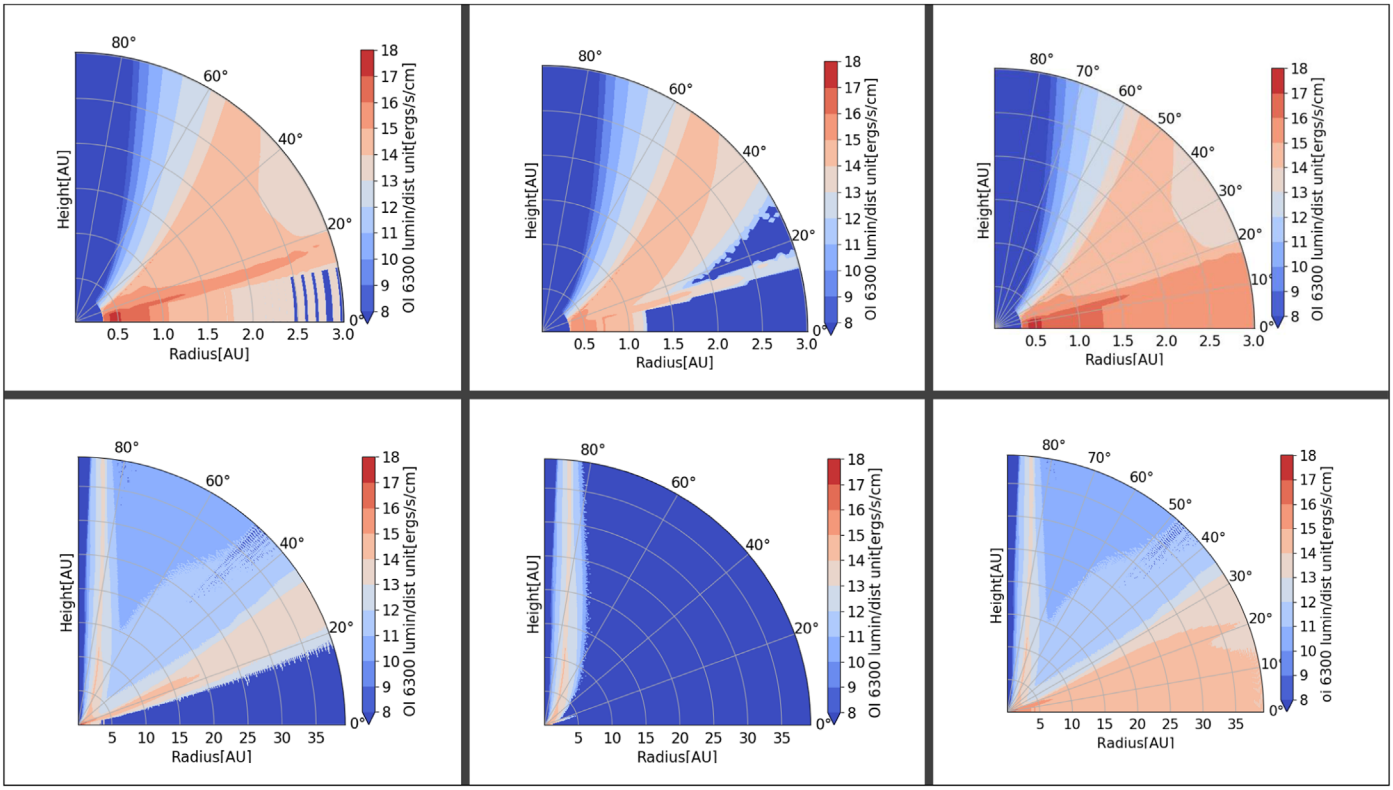

Figure 2. Polar plots for [O I] 6300 Å luminosity using EO16's hydrodynamical model, zoomed into 3au, for three cases: The 0.1 μm grain model with pumping (left column); the corresponding model without pumping (middle column); and the grain-free model (right column). The luminosity per unit radial distance was produced by differencing the cumulative luminosity output by Cloudy, leading to some numerical noise.

equations.) Moreover, the luminosities of the O I 6300 and 5577 Å lines drop by 94% and 98%, respectively, as can be seen in Table 1. The ratio of the lines doubles to resemble the models that did not match the observed luminosity previously. The exception is the grain-free model. In that model we are able to produce the observed luminosity, and the majority of the emission, in addition to the above mentioned regions, comes from the disk midplane (Figure 2), which is due to the complete lack of absorption of the FUV by the dust grains that otherwise would be concentrated in the disk midplane. This also explains why depleting the dust caused an increase in the forbidden-line luminosities.

To verify the effect of the ultraviolet (UV) on the radiation-transfer solutions, we reduce the luminosity of the two FUV sources (stellar and accretion) by an order of magnitude, while maintaining the X-ray luminosity. The ionization fraction does not change much throughout the wind, although the ionization front recedes inward toward the star. The luminosity of the [O I] 6300 Å line is reduced by 87%. Moreover, the assumption that the accretion FUV source can be modeled as a blackbody is questionable, and it is expected that the FUV pumping will depend sensitively upon the assumed blackbody temperature. To test this dependence, we ran a simulation with our base model and changed T(BB) from 12,000 to 9000 K; and the luminosity of the lines dropped by ∼80%. The emission from disk diminishes in both of these tests in much the same way as when we disabled FUV pumping entirely.

In addition to thermal accommodation with the gas, dust grains absorb FUV radiation and re-emit it in the infrared, as is evident by the correlation between infrared and FUV emission from YSOs (Rigliaco et al. 2013). We traced the different types

Table 1
Results from Radiative Transfer Using Owen et al. (2010) and Wang et al. (unpublished) Hydrodynamical Models Using 0.1 μm Grains

Results	Owen's Model	Wang's Model
[O I] 6300 Å luminosity (L_{sol})	3.6×10^{-5}	7.36×10^{-5}
[O I] 6300 Å luminosity no pump (L_{sol})	2.17×10^{-6}	5.25×10^{-5}
O I 5577 A luminosity (L_{sol})	2.8×10^{-6}	3.04×10^{-6}
O I 5577 A luminosity no pump(L_{sol})	3.2×10^{-8}	7.65×10^{-7}
O I 6300/5577 ratio	13.5	24.2
O I 6300/5577 ratio no pump	66.0	68.6

of radiation (infrared (IR), FUV, EUV, and X-ray) as a function of distance from the star for certain directions in 1D simulations to understand the effect of dust on them. In all dust models mentioned above, the EUV radiation suffers from a significant drop at the ionization front (where all of the radiation is absorbed to ionizing the hydrogen and oxygen atoms) and the [O I] 6300 Å emission peaks at that same point as discussed above. In the models where FUV pumping did not have a significant effect on the O I line emission, the FUV was quickly (<5 au) converted into IR due to absorption and thermal emission by dust grains, and the [O I] 6300 Å emission drops significantly beyond the peak that coincides with the ionization front. On the contrary, in the models where FUV pumping played a key role in the O I line emission, the FUV was radially constant in those regions with significant O I emission, and had a higher luminosity than the IR. To confirm this result we had the code output the dominant processes for the various predicted lines, and it reported that all the neutral oxygen lines between 930 and 1350 Å were predominantly

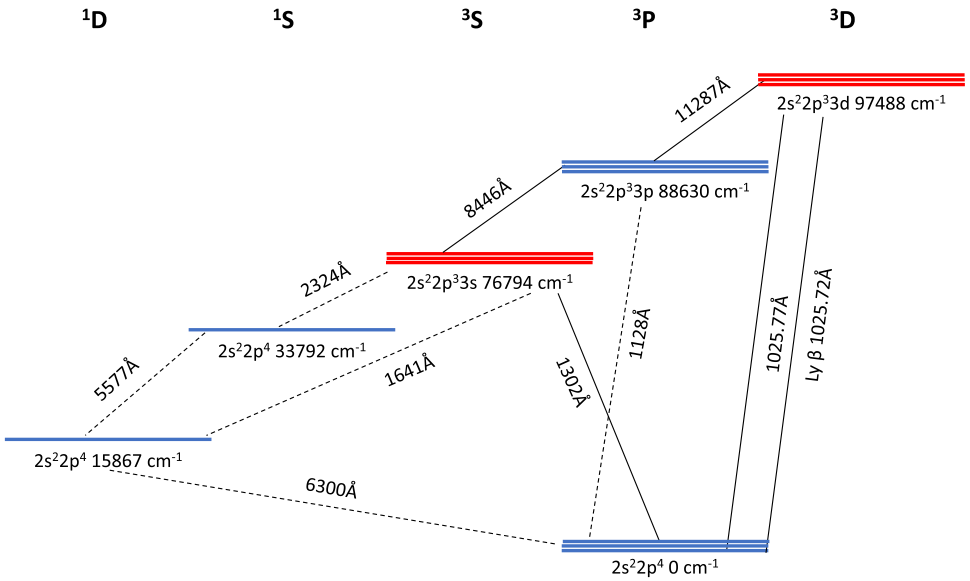

Figure 3. Grotrian diagram of the oxygen atom including important levels for FUV pumping of the O I forbidden lines. The terms are specified on the top, and the wavenumber of every level is specified below it with the configuration. The transitions connecting these levels are classified as permitted (solid) or semi-forbidden/forbidden (dashed) with the wavelength noted on each line. The levels highlighted in red have the highest probability of reaching the upper states of the forbidden lines if pumped by continuum or Lyβ FUV photons.

populated through FUV pumping by the FUV radiation (i.e., those lines are optically thick). The effect of this absorption is changing the population of the all the excited levels of neutral oxygen, which in turn will change the emissivities of the O I 6300 and 5577 Å probably in different proportions.

In Figure 3 we show a Grotrian diagram of the O atom for 14 levels (or seven terms) to demonstrate the effect of FUV pumping. We constructed an atomic model for the first 29 levels of the oxygen atom and included radiative and collisional transitions between them to study the probability that an atom excited to any of those levels by absorption of UV would end up in the upper states of the forbidden transitions. Under optically thin conditions, allowed transitions to the ground state are strongly favored over forbidden or semi-forbidden transitions to the upper states of the forbidden lines; the product of branching ratios leading to the latter states is negligible (a few parts in a million). But when we included the effects of optical depth at the physical conditions of the emitting region ($n_{\rm h} \sim 10^7\,{\rm cm}^{-3}$, column density $N_h \sim 10^{20}\,{\rm cm}^{-2}$, implying an optical depth $\sim$400 for the permitted transitions) we found that the triplet at 76794 cm^{-1} has a significantly higher probability ($\sim$3%) to contribute to the forbidden lines. (A photon emitted in a permitted downward transition is usually promptly absorbed by another oxygen atom, effectively undoing the transition; but it may escape instead, with a probability inversely proportional to the optical depth at line center.) That is, a few percent of the continuum FUV photons resonant with those levels (1304Å) will pump atoms from the ground that cascade through the upper states of the [O I] 6300 Å and 5577 Å lines before returning to ground, thereby producing the forbidden lines. Moreover, Lyβ is coincident in energy with a permitted O I line connecting the ground to the triplet at 97488 cm^{-1}; thus Lyβ line can also pump the [O I] lines. This is famously known as the Bowen mechanism. Our Cloudy simulations show that the equivalent width of Lyβ relative to the total FUV continuum (incident from the source plus diffuse) in the pumped regions of the disk is modest ($\approx$0.1 Å). Nevertheless, as a result of optical depth effects, the branching ratio to the upper states of the [O I] lines is $\gtrsim$1%. The effect of FUV pumping on the forbidden-line luminosities has been observed before (Dupree et al. 2016), as will be further discussed in Section 3.

EO16 argued that much of the [O I] 6300 Å emission comes from regions where collisions with atomic hydrogen rather than electrons dominate the excitation of the upper state. Such regions would need to have ionization fractions $<10^{-3}$ to balance the much higher ($>10^3$) collisional rate coefficients of electrons (Simon et al. 2016). As can be seen from Figure 1, the emission comes from regions where the ionization fraction is significantly higher than 10^{-3}; EO16 reported emission from similar spatial regions. In addition, the ionization thresholds and the photoionization cross sections of neutral oxygen and hydrogen are similar, so we expect the gas to have insufficient neutral hydrogen to dominate the excitation of the [O I] lines. EO16 and Cloudy use collision data with neutral hydrogen from the literature for the [O I] 6300 Å line (Launay & Roueff 1977; Krems et al. 2006), respectively. In addition, Cloudy includes an approximation for neutral H collision rate for the [O I] 5577 Å line (Kiselman 2001), while EO16 did not. EO16 switched off the neutral H collisions for the [O I] 6300 Å line and found that the line luminosity dropped by a factor of 3, causing a drop in the ratio of [O I] lines by the same factor to match the observed ratio. We found that switching off collisions with neutral hydrogen had a negligible effect on the total luminosity of the [O I] 6300 and 5577 lines: their luminosities dropped by only 2.5% and $<$1%, respectively.

2.1. Magnetothermal Wind

To test the sensitivity of FUV pumping to the density and temperature structure of the disk and wind, we have made a similar analysis for (heretofore unpublished) magnetothermal wind models like those of Wang et al. (2019) but extended to smaller radii in an attempt to confirm the role of FUV pumping on the O I forbidden lines (Figure 4). As this Letter is

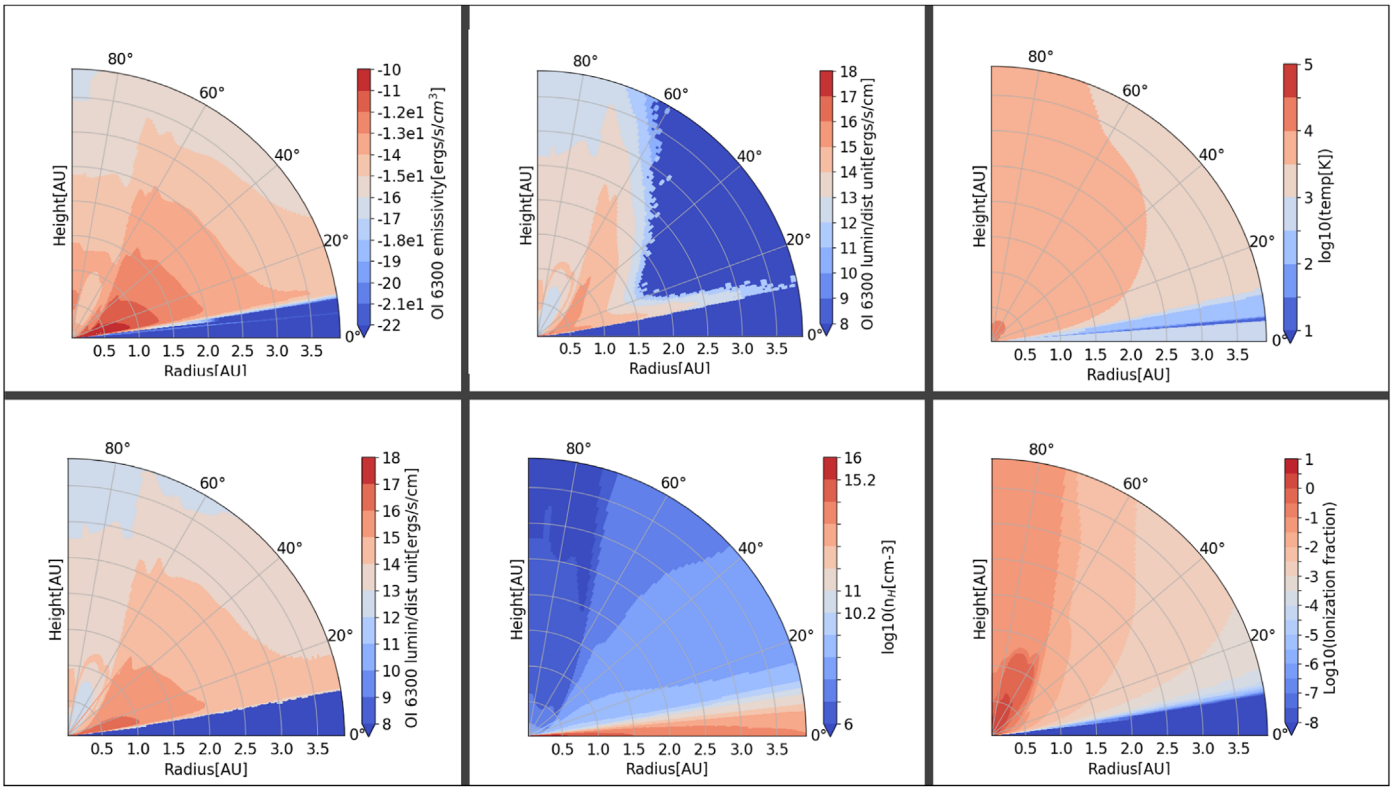

Figure 4. Polar plots of luminosity per distance for [O I] 6300 Å for cases with (bottom-left panel) and without (top-middle panel) FUV pumping, along with the ionization fraction, temperature, and density in Cloudy calculations applied to new MHD-wind models like those of Wang et al. (2019) but focused on $r \leqslant 5$ au.

concerned mainly with studying the excitation mechanisms of the O I forbidden lines, we chose to use the same input parameters (radiation sources, dust size, and abundance) as used above for EO16 hydrodynamical model when post-processing Wang et al.'s model. Hence, as with EO16's model, the post-processed temperature and ionization differ from somewhat from those in the dynamical calculation. We use the same elemental abundances as reported by Wang et al. (2019) and we include dust and molecules in the model as in our fiducial model. The gas starts at the surface of the star at $r = 1.74 \times 10^{11}$ cm and ends at $r = 4$au. The density profile that was fed to these Cloudy models was extracted from the results of the MHD models computed following the work of Wang et al. (2019). We conducted further simulations to investigate the innermost regions. The schemes of these simulations is largely inherited from Wang et al. (2019), with a few additions to account for processes taking place in the innermost disk. The updated thermochemical network includes K and K^+ (potassium and the positive ion) and their related reactions, especially collisional ionization that are believed to dominate the ionization of inner disk regions. The simulation has 240 × 144 resolution for the 2.5D axisymmetric spherical polar grid covering grid $r \in [0.2\ \mathrm{au}, 4\ \mathrm{au}]$ and $\theta \in [0.06, \pi/2]$, respectively. The radial zones are spaced logarithmically, and the latitudinal zones are spaced in such a way that there are ∼10 zones per scale height near the equatorial plane. Other numerical and physical conditions, including boundary and initial conditions of the disk and the fields, stellar properties, and high-energy radiation luminosities, are set up in the the same way as Wang et al. (2019).

We adopt the simulation results to study the effect of FUV pumping on the [O I] 6300 and 5577 Å lines: the first case that includes the above parameters; the second case where we switch off FUV pumping for the base model. The results of these simulations are reported in Table 1. As can be seen, the FUV pumping has a significant effect on the line luminosities.

3. Discussion

As can be seen from the results reported in the previous section, it is evident that the [O I] 6300 Å:[O I] 5577 Å emission is significantly affected by thermal excitation, but we showed for the simulations based on EO16's model that collisions are not the dominant excitation mechanism. Moreover, the conditions for neutral-hydrogen collisions to dominate over electron collisions are not available in the emitting regions reported here.

We noticed that the thermal emission in both cases comes from similar regions along the ionization front. Also, in both models, FUV pumping is most important near the surface of the disk.

In both wind models (the photoevaporative wind of EO16 and the new magnetothermal wind), we find that FUV pumping affects the [O I] 6300 Å:[O I] 5577 Å emission appreciably. Using the Owen et al. (2010) model, we find that FUV pumping dominates the line emission (∼90%) and that the thermal excitation is only a small fraction of that. In contrast, for the denser magnetothermal model, thermal excitation dominates [O I] 6300 Å (∼80%) but not [O I] 5577 Å (∼25%); nevertheless, FUV pumping is significant for both lines.

Under optically thin conditions, the branching ratios of allowed O I transitions are significantly higher than those of forbidden or semi-forbidden transitions. But at hydrogen columns $\gtrsim 10^{20}\ \mathrm{cm}^{-2}$, the photons associated with the

permitted transitions are absorbed and re-emitted many times before escaping. The trapping of those photons increases the effective branching ratios of the semi-forbidden transitions, in particular those that lead to the upper levels of the [O I] lines.

Moreover, Lyβ pumping of the O atom is well known in the literature to have a significant effect on the O I spectrum (Kastner & Bhatia 1995); unfortunately we are unaware of previous studies of this for optically thick conditions. UV surveys document the dominating strength of the O I resonance lines in cool luminous stars (Ayres et al. 1995) and require the inclusion of photoexcitation and photoionization from hydrogen radiation in the calculation of oxygen level populations and ionization. This effect was also observed by Dupree et al. (2016). They showed that the forbidden O I lines (which had been thought to be analyzed correctly with local thermal equilibrium (Kiselman 2001)) are changed drastically when Bowen fluorescence (absorption of Lyβ by atomic oxygen) is accounted for. Mathew et al. (2018) also showed that Bowen fluorescence is likely to be more important than collisional excitation for the O I spectra of Herbig stars.

Electron collisions and FUV pumping are not the only processes that may excite the forbidden oxygen lines. As noted in Section 1, Gorti et al. (2011) and Rigliaco et al. (2013) have suggested that photodissociation of OH may be important and would naturally produce the line ratio 6300: 5700 $\approx$ 7:1 as observed. Fang et al. (2018) have argued against this on the grounds that the [S II] 4068 Å line shows similar velocity structure to that of the [O I] lines and is collisionally excited under similar conditions. Gorti et al. (2011) made this suggestion in the context of their analysis of TW Hya, which shows a negligible blueshift: in this system, the oxygen lines presumably come from the disk. If there are other systems in which OH dissociation dominates the [O I] luminosity and occurs mainly in the wind, rather than the disk, comparison with likely wind mass-loss rates shows that OH would have to re-form many ($\sim$100 times) in the wind. We have made simple estimates indicating that the required reformation rates are plausible, but we have not made a systematic study of the contribution of OH dissociation to the [O I] lines in either of the wind models discussed in this Letter.

4. Conclusion

We have presented the results of radiation transport simulations, using Cloudy, for two dynamical protoplanetary-disk models; an X-ray driven photoevaporative wind due to Owen and collaborators, and a magnetothermal model similar to those of Wang et al. (2019). We found that FUV pumping has a dominant effect on the [O I] 6300 Å and [O I] 5577 Å lines in the former model, and a weaker, yet significant, effect in the latter, which is denser. FUV pumping causes a general increase in the level populations of the oxygen atom, and that increase is dependent on the local physical conditions of the emitting region. In agreement with previous calculations, thermal excitation dominates near ionization fronts, which are found at high latitudes in both of these models. As a result, we expect that the consideration of FUV pumping in the radiation transport simulations will significantly affect the strengths and shapes of the [O I] 6300 Å and [O I] 5577 Å lines. It is not clear yet whether these lines can be used as tracers of disk winds in protostellar disk environments. The utility of these and other lines for distinguishing hydrodynamic from MHD wind models is a question that we leave for future work.

We thank James Owen and Barbara Ercolano for sharing unpublished details of their work, Edward Jenkins and Bruce Draine for advice on atomic processes, and Gary Ferland for help with Cloudy. This work was supported by NASA grant 17-ATP17-0094.

ORCID iDs

Ahmad Nemer https://orcid.org/0000-0002-9220-0039
Jeremy Goodman https://orcid.org/0000-0002-6710-7748
Lile Wang https://orcid.org/0000-0002-6540-7042

References

Alexander, R., Pascucci, I., Andrews, S., Armitage, P., & Cieza, L. 2014, in Protostars and Planets VI, ed. H. Beuther et al. (Tucson, AZ: Univ. Arizona Press), 475
ALMA Partnership, Brogan, C. L., Pérez, L. M., et al. 2015, ApJL, 808, L3
Ayres, T. R., Fleming, T. A., Simon, T., et al. 1995, ApJS, 96, 223
Baldovin-Saavedra, C., Audard, M., Carmona, A., et al. 2012, A&A, 543, A30
Beristain, G., Edwards, S., & Kwan, J. 2001, ApJ, 551, 1037
D'Alessio, P., Calvet, N., Hartmann, L., Franco-Hernández, R., & Servín, H. 2006, ApJ, 638, 314
Dupree, A. K., Avrett, E. H., & Kurucz, R. L. 2016, ApJL, 821, L7
Ercolano, B., & Owen, J. E. 2016, MNRAS, 460, 3472
Ercolano, B., & Pascucci, I. 2017, RSOS, 4, 170114
Fang, M., Pascucci, I., Edwards, S., et al. 2018, ApJ, 868, 28
Ferland, G. J., Chatzikos, M., Guzmán, F., et al. 2017, RMxAA, 53, 385
Ferreira, J. 2013, in Role and Mechanisms of Angular Momentum Transport During the Formation and Early Evolution of Stars, EAS Publications Series, Vol. 62, ed. P. Hennebelle & C. Charbonnel (Les Ulis: EDP), 169
Frank, A., Ray, T. P., Cabrit, S., et al. 2014, in Protostars and Planets VI, ed. H. Beuther et al. (Tucson, AZ: Univ. Arizona Press), 451
Gorti, U., Hollenbach, D., Najita, J., & Pascucci, I. 2011, ApJ, 735, 90
Güdel, M., Dvorak, R., Erkaev, N., et al. 2014, in Protostars and Planets VI, ed. H. Beuther et al. (Tucson, AZ: Univ. Arizona Press), 883
Hartigan, P., Edwards, S., & Ghandour, L. 1995, ApJ, 452, 736
Kastner, S. O., & Bhatia, A. K. 1995, ApJ, 439, 346
Kiselman, D. 2001, NewAR, 45, 559
Konigl, A., & Pudritz, R. E. 2000, in Protostars and Planets IV, ed. V. Mannings, A. P. Boss, & S. S. Russell (Tucson, AZ: Univ. Arizona Press), 759
Krems, R. V., Jamieson, M. J., & Dalgarno, A. 2006, ApJ, 647, 1531
Launay, J. M., & Roueff, E. 1977, A&A, 56, 289
Lynden-Bell, D., & Pringle, J. E. 1974, MNRAS, 168, 603
Mathew, B., Manoj, P., Narang, M., et al. 2018, ApJ, 857, 30
Natta, A., Testi, L., Alcalá, J. M., et al. 2014, A&A, 569, A5
O'dell, C. R., & Wen, Z. 1994, ApJ, 436, 194
Owen, J. E., Ercolano, B., Clarke, C. J., & Alexander, R. D. 2010, MNRAS, 401, 1415
Pascucci, I., & Sterzik, M. 2009, ApJ, 702, 724
Rigliaco, E., Pascucci, I., Gorti, U., Edwards, S., & Hollenbach, D. 2013, ApJ, 772, 60
Sacco, G. G., Flaccomio, E., Pascucci, I., et al. 2012, ApJ, 747, 142
Shu, F. H., Najita, J. R., Shang, H., & Li, Z. Y. 2000, in Protostars and Planets IV, ed. V. Mannings, A. P. Boss, & S. S. Russell (Tucson, AZ: Univ. Arizona Press), 789
Simon, M. N., Pascucci, I., Edwards, S., et al. 2016, ApJ, 831, 169
Turner, N. J., Fromang, S., Gammie, C., et al. 2014, in Protostars and Planets VI, ed. H. Beuther et al. (Tucson, AZ: Univ. Arizona Press), 411
van Boekel, R., Güdel, M., Henning, T., Lahuis, F., & Pantin, E. 2009, A&A, 497, 137
Wang, L., Bai, X.-N., & Goodman, J. 2019, ApJ, 874, 90
Weber, M. L., Ercolano, B., Picogna, G., Hartmann, L., & Rodenkirch, P. J. 2020, MNRAS, 496, 223